Review article

Jitter solution in parameter identification based on cross-time scale fusion algorithm of lithium-ion batteries

Xianzheng Su [a], Yanjun Ge [a,*], Xin Qiao [b]

[a] *School of Mechanical Engineering, Dalian Jiaotong University, 116028, Dalian, China*
[b] *School of Rail Transportation, Shandong Jiaotong University, 250357, Jinan, China*

ARTICLE INFO

ABSTRACT

Accurate state-of-charge (SOC) estimation is the core index of battery management system (BMS). When the battery equivalent circuit model (ECM) identifies the parameters under complex operating conditions, there is more jitter or even divergence, which will affect the estimation accuracy of battery SOC. To solve this problem, this paper proposes a new algorithm, namely the cross time scale fusion (CTSF) algorithm. Firstly, the cross-time scales Δt_1 and Δt_2 are determined, the number of cross-time cycles is calculated according to the total amount of complex operating condition data N. Then the ECM parameters are identified in Δt_1 by using forgetting factor recursive least square (FFRLS), and the battery SOC is estimated in Δt_2 based on the identified parameters, finally the battery parameters are identified and the SOC is estimated by cycling in the cross-time. The experimental results show that, no matter at the same temperature in different conditions or at different temperatures in the same condition, The proposed algorithm not only effectively solves the ECM parameter identification jitter problem, but also improves the accuracy of SOC estimation, the Mean Absolute Error (MAE) minimum of SOC result is 1.42% for different operating conditions at the same temperature and 0.25% for different temperatures at the same operating conditions, respectively.

1. Introduction

Electric vehicles (EVs) are increasingly recognized as an effective solution for reducing greenhouse gas emissions and improving energy efficiency [1,2]. Lithium-ion batteries are a preferred energy source due to their high energy density, capacity, service life, low loss, and self-discharge rate [3]. However, lithium-ion batteries have certain limitations, such as aging in use and sensitivity to high temperatures [4]. Therefore, an advanced BMS plays a critical role in monitoring temperature changes and predicting aging effects [5].

In addition, accurate battery modeling is essential for SOC estimation, regular models including electrochemical models, data models, data-driven models, ECM, etc. [6–8]. While electrochemical models require prior acquisition of electrochemical dynamic parameters, these parameters are commonly used to understand internal battery reaction processes, facilitate battery design, and optimize production [9]. Data-driven models also have limitations. In particular, they lack interpretability and are sensitive to data quality [10]. However, ECM has been widely adopted for SOC estimation due to its advantages of fast execution speed, simplicity, and relatively high accuracy [11]. Researchers have explored various methods in the literature for SOC estimation based on the ECM

Table 1
Comparison of the SOC errors.

Review article	Type of model	Metric
[24]	Equivalent Circuit Model	MAE < 2%
[25]	Equivalent Circuit Model	Maximum Error < 2.5%
[26]	Data-driven models	RMSE < 1.78%
[27]	Data-driven models	MAE < 1.5%
[28]	Data-driven models	MAE < 1.5%
[29]	Equivalent Circuit Model	MAE < 1.3%

[12]. An adaptive unscented Kalman filter (AUKF) based on an accurate ECM is proposed in [13] to improve the SOC estimation. The accuracy advantage of the n-RC model is proved, the accuracy of the extended Kalman filte(EKF) and AUKF algorithms were compared, experimental results showed that the AUKF algorithm achieved higher accuracy. In [14], the combination of Decoupled Recursive Least Squares (RLS) technique and Time-Domain Parameter Extraction enables both ECM parameter estimation, In addition, a compensation term for DC resistance is proposed, which greatly improves the accuracy of SOC estimation. In [15], a novel Adaptive Extended Kalman Filter (AEKF) combined with a parameter identification algorithm RLS is introduced as another SOC estimation method, the tests demonstrate the accurate estimation of battery SOC and the robustness.

Currently, there have been several advances in battery SOC estimation. Chen [16] proposed an improved machine learning (ML) model-based method for SOC estimation. The method uses an AhI-based constraint strategy to smooth the network output SOC. Fazel [17]proposed a mathematical model for SOC of a Li-ion battery using the improved Coulomb counting (iCC) algorithm and decadal uncertainty assessment. The maximum estimation error using the proposed method is 0.3%. Wang [18] proposed an improved gated recurrent unit (GRU)-based transfer learning method for estimating SoC with small target sample sets. The method includes an improved GRU hidden unit structure and integration with transfer learning. Ren [19] proposes a long short-term memory neural network based on particle swarm optimization (PSO-LSTM). The experiments demonstrate that the proposed method has an error rate of only 0.5%. Feng [20] proposed the Clockwork Recurrent Neural Network (CWRNN) structure, which performs computations in a defined number of clock cycles, reducing training and computation costs. Experiments show an root mean square error (RMSE) of less than 1.29%.

Parameter estimation in lithium battery ECMs under filtering algorithms is challenging due to the large number of parameters to be estimated while the observed signals are typically limited to voltage and current. It is important to develop a method that can solve this problem, especially under complex operating conditions. Several studies have been conducted on this topic. For instance, Ge et al. proposed an improved joint algorithm for the forgetting factor recursive least squares extended Kalman filter, which eliminates jitter, even negative values, during online identification of battery model parameters [21]. Chen et al. proposed a new parameter identification method with a parameter backtracking strategy that significantly reduces parameter jitter during the Open Circuit Voltage (OCV) identification procedure [22]. Wang et al. analyzed the parameter identification methods for ECM and found that the Forgetting Factor Recursive Least Square (FFRLS) method is unable to track parameter changes, resulting in abnormal parameter fluctuations. To address this issue, they proposed an alternative method called Generalized Least Squares with Forgetting Factor (FF-AGLS) [23]. The identification of ECM parameters often faces the challenge of jitter or even divergence. Therefore, finding suitable algorithms to eliminate the jitter is essential.

To address the previously mentioned issue, we propose a new method to eliminate parameter identification jitter and improve battery SOC estimation accuracy. The main contributions of this article are:

(1) The article analyzes the ECM and open circuit voltage models of lithium batteries. Ultimately, the second-order equivalent circuit model is chosen to ensure accurate parameter identification.

(2) The cross-time scale fusion algorithm proposes a new method for identifying Li-ion battery parameters and SOC. The algorithm determines the interval of parameter identification time scale Δt_1, and SOC estimation time scale Δt_2. By cross-estimating the battery parameters and SOC within complex battery conditions, the algorithm reduces parameter jitter and improves SOC estimation accuracy.

(3) The experiment analyzes the accuracy of parameter identification and SOC estimation under different operating conditions at the same temperature and different temperatures at the same operating condition. The results demonstrate the superiority of the proposed algorithm.

The rest of the paper is organized as follows: Section 2 establishes the lithium battery model, including the ECM and OCV model. Section 3 analyzes the novel proposed algorithm, presents the CTSF algorithm and determines the value of cross-time scale. Section 4 presents experimental validation followed by discussion of the results and comparison of the evaluated methods. Finally, conclusions are drawn in section 5.

2. Related work

Estimation of SOC for lithium batteries has been studied many years ago, Table 1 gives a comparison of the SOC errors in recent years.
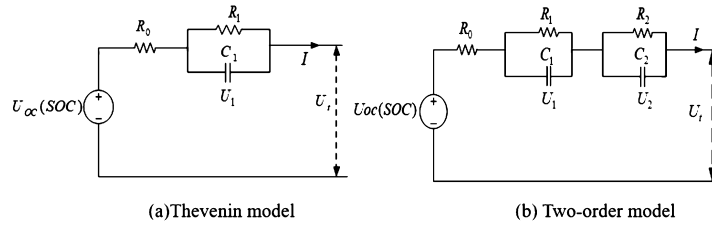
Fig. 1. Description of ECM.

2.1. ECM for lithium-ion battery

The accurate estimation of battery SOC relies heavily on the establishment of a high-precision battery model [30]. In addition, the computational complexity of the ECM increases with the number of parameters used [31]. So, considering the computational complexity and accuracy requirements, widely used ECMs include the Thevenin model and the second-order RC model, as shown in Fig. 1.

From Fig. 1, $U_{oc}(SOC)$ is the open circuit voltage, U_t is the terminal voltage, R_0 is the ohmic internal resistance, R_1, R_2 is the polarization internal resistance, and C_1, C_2 is the polarization capacitance, U_1, U_2 is the polarization voltage. Based on Kirchhoff's circuit laws, the electrical relationship of the Thevenin model can be derived as follows:

$$\begin{cases} I(t) = C_1 \dfrac{dU_1(t)}{dt} + \dfrac{U_1(t)}{R_1} \\ U_{OC}(SOC(t)) = U_t(t) + I(t)R_0 + U_1(t) \end{cases} \tag{1}$$

Similarly, two-order model can be derived as follows:

$$\begin{cases} I(t) = C_1 \dfrac{dU_1(t)}{dt} + \dfrac{U_1(t)}{R_1} \\ I(t) = C_2 \dfrac{dU_2(t)}{dt} + \dfrac{U_2(t)}{R_2} \\ U_{OC}(SOC(t)) = I(t)R_0 + U_1(t) + U_2(t) + U_t(t) \end{cases} \tag{2}$$

The models mentioned above accurately represent the dynamic and static characteristics of lithium batteries while balancing complexity and practicality, making them suitable for engineering applications. However, the second-order ECM provides higher accuracy. Therefore, considering the need for accurate parameter identification of the ECM under complex operating conditions, the second-order model was selected for this study.

2.2. OCV model

The SOC-OCV curve is generally defined as the voltage difference between the positive electrode (PE) and the negative electrode (NE) of a battery [32]. This measurement is made at different SOC points when the battery system is in a state of equilibrium without any current flow [33]. Within the battery ECM, the SOC-OCV curve holds significant importance as a key parameter that significantly affects the accuracy of SOC estimation. Therefore, obtaining an accurate SOC-OCV function is critical to achieving accurate SOC estimation. This serves as the fundamental basis for ensuring high accuracy in SOC estimation.

Furthermore, in the quest for accurate SOC estimation, researchers have developed various methods to obtain the SOC-OCV curve. Among these methods, galvanostatic intermittent titration (GITT) and pseudo-OCV are commonly used. GITT involves specific charge-discharge steps and carefully timed rest periods that are essential to achieve equilibrium. During the quiescent period, no current flows through the battery, allowing sufficient time for the system to stabilize. To improve the accuracy of the SOC-OCV curve, it is imperative to use finer charge-discharge steps and longer rest periods. On the other hand, pseudo-OCV uses small charge or discharge currents, such as C/25, C/40 or even lower, to record the SOC-OCV curve. Each method has its own unique requirements and considerations to ensure accurate SOC estimation, and to better describe the true OCV curve, researchers have proposed a number of models, ranging from simple linear approximations to polynomial and exponential models, among others. Table 2 provides an overview of some typical OCV curve models [34]. The primary goal of these models is to provide a more accurate representation of the real OCV curve.

Fig. 2 displays the SOC-OCV fitting curves obtained using the pseudo-OCV method for the A123 lithium-ion battery data set from the Center for Advanced Life Cycle Engineering (CALCE) at the University of Maryland at a temperature of 25 °C [35]. The figure indicates that the 6th order polynomial model has lower fitting accuracy compared to the 9th and 12th order polynomial models. Conversely, the 12th order polynomial model exhibits signs of overfitting. Therefore, based on the comparison, the 9th order polynomial model is selected to fit the SOC-OCV curve, and the fitting formula is:

Table 2
Overview of OCV model.

OCV curve fitting formula	RMSE	Complexity
$OCV(x) = K_0 + K_1 \ln(x) + K_2 \ln(1-x)$	0.0433	110
$OCV(x) = K_0 + \frac{K_1}{x} + K_2 x + K_3 \ln(x) + K_4 \ln(1-x)$	0.0268	130
$OCV(x) = K_0 + \frac{K_1}{x} + \ldots + \frac{K_4}{x^4} + K_5 x + K_6 \ln(x) + K_7 \ln(1-x)$	0.0108	160
$OCV(x) = K_0 + K_1 x + \ldots + K_m x^m$	0.0202	60
$OCV(x) = K_0 + K_1 e^x + K_2 e^{x^2} + \ldots + K_m e^{x^m}$	0.0160	260
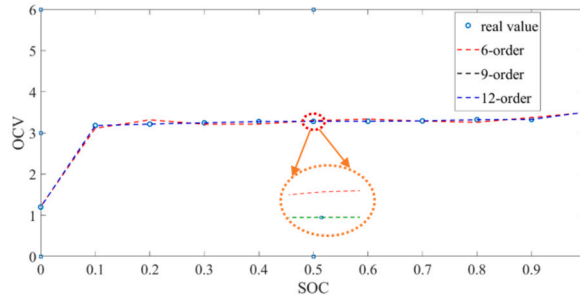
Fig. 2. SOC-OCV fitting curves under different orders.

Table 3
Framework of proposed algorithm.

Algorithm 1 proposed algorithm
01: input: $\theta = \theta_{initial}$, $x = x_{initial}$, $P = P_{initial}$, $\lambda = \lambda_{initial}$
02: Identification of battery parameters within the time interval scale Δt_1
03: Estimate battery SOC within time scales interval Δt_2
04:for m = 0 to z_s -1 do
05:    for t = 1+m* z_s to Δt_2 + m* z_s do
06:        Calculate the ECM parameters $R_0 \sim C_2$
07:    end for
08:    for k = 1+m* z_s to Δt_1 + m* z_s do
09:        Estimate SOC of the battery
10:    end for
11:    m = m+1
12:    if (m $< z_s$ -1)
13:        Repeat steps 4 to 14
14:    end for
15:    else
16:        Output parameter identification and SOC results
17:end for

$$OCV = 2820 SOC^9 - 1.37e^4 SOC^8 + 2.863e^4 SOC^7$$
$$-3.366e^6 SOC^6 + 2.442e^4 SOC^5 - 1.125e^4 SOC^4 \tag{3}$$
$$+3259 SOC^3 - 565.7 SOC^2 + 52.88 SOC + 1.2$$

3. Proposed method

This section presents a new algorithm for identifying battery parameters and estimating SOC. It first outlines the algorithm's framework and then describes the specific computational process of the CTSF algorithm.

3.1. Framework of the proposed algorithmic

The process for identifying parameters and estimating SOC using the CTSF algorithm is outlined in Fig. 3. A more detailed explanation of the algorithm can be found in Table 3.

3.2. Detailed procedure of the proposed algorithm

In step 1 of Fig. 3, it is first necessary to determine the values of the two cross-time scales Δt_1 and Δt_2, identify the equivalent circuit model parameters in Δt_1, feed the identification results to Δt_2, and estimate the battery SOC in Δt_2.

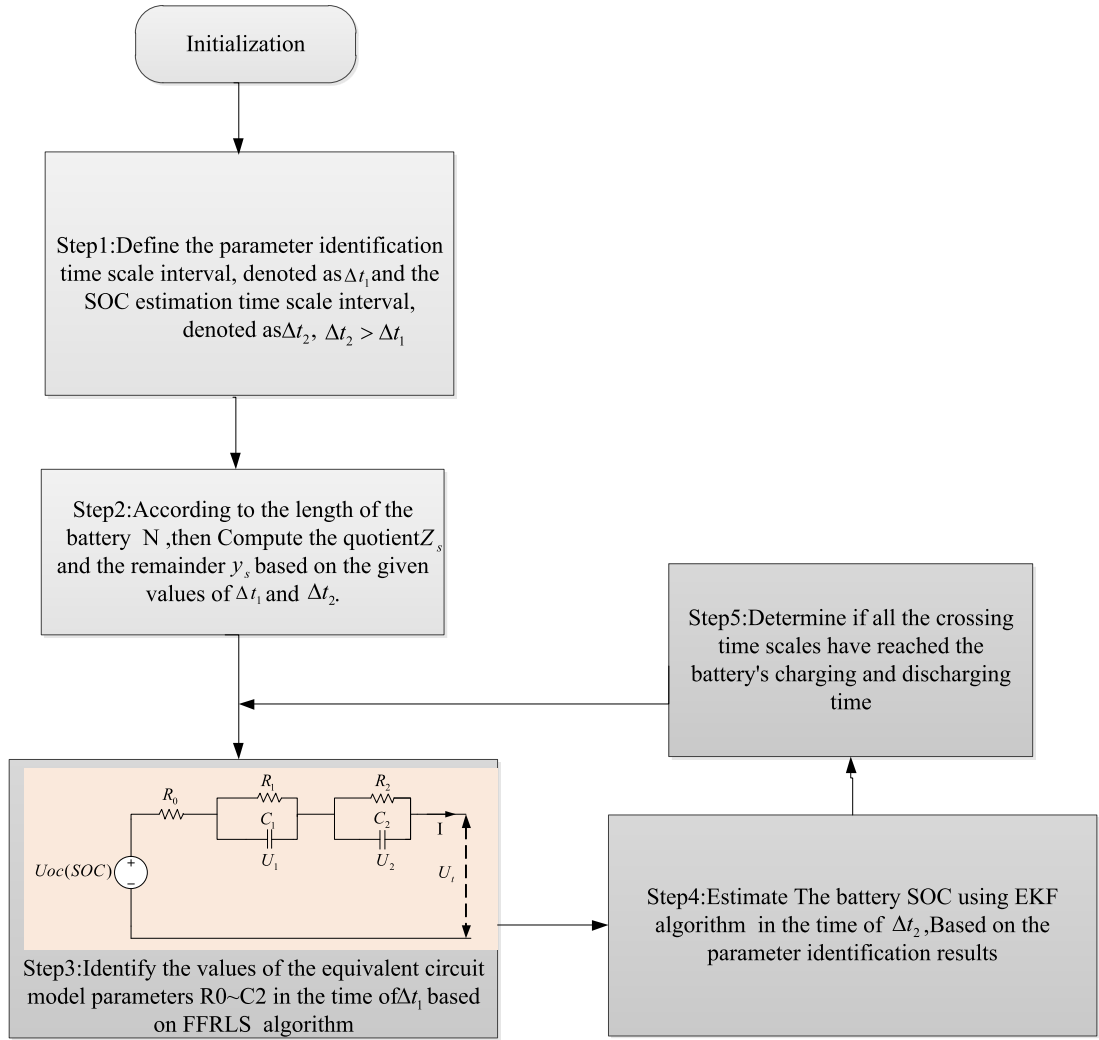**Fig. 3.** Framework of proposed algorithm.

In step 2, we need to calculate the cycle identification number Z_s according to the total battery charge/discharge data volume N and the cross time scale Δt_1, Δt_2, which lays the foundation for the subsequent realization of the identification in the cross-time scale.

In step 3, the battery ECM parameters need to be identified using FFRLS within the time scale interval Δt_1, which is calculated as follows:

According to the Fig. 1, the electrical relationship of ECM is expressed in s domain:

$$G(s) = \frac{U_t(s) - U_{oc}(s)}{I(s)} = -(R_0 + \frac{R_1}{1 + \tau_1 s} + \frac{R_2}{1 + \tau_2 s}) \tag{4}$$

In Equ. (4), s is the Laplacian in s domain, time constant $\tau_1 = R_1 C_1$ and $\tau_2 = R_2 C_2$. By simplifying the Equ. (4), we can get the values of the parameters R_0, R_1, R_2, C_1 and C_2.

$$\begin{cases} R_0 = a \\ R_1 = \dfrac{\tau_1(d-a) + ac - f}{\tau_1 - \tau_2} \\ R_2 = d - a - R_1 \\ C_1 = \dfrac{\tau_1}{R_1} \\ C_2 = \dfrac{\tau_2}{R_2} \end{cases} \tag{5}$$

In step 4, the battery SOC is estimated using EKF within the time scale interval Δt_2 as follows:

For a nonlinear discrete system, the equations of state and observation are as follows:

$$\begin{cases} x_{k+1} = f(x_k, u_k) + w_k \\ y_k = g(x_k, u_k) + v_k \end{cases} \tag{6}$$

In Equ. (6), x_k is the state variable of the system at moment k, u_k is the input variable of the system at moment k, y_k denotes the output of the system at the moment of k, w_k and v_k denote the process noise and observation noise of the system, respectively, which are Gaussian white noises independent of each other, and their process and observation noise covariances are Q, R.

The nonlinear system equations $f(x_k, u_k)$, $g(x_k, u_k)$ of Eq. (6) are expanded in Taylor series, removing the higher terms and retaining the primary terms to obtain an approximate linear system. The linear equation of state is as follows:

For nonlinear functions $f(x_k, u_k)$ and $g(x_k, u_k)$, the Taylor series expansion is employed to approximate them by retaining the first-order derivative terms and constant terms. This enables the transformation of the nonlinear functions into linear functions.

$$x_{k+1} = A_k x_k + B_k u_k + w_k \tag{7}$$

where the matrix of each parameter is defined as:

$$\begin{cases} A_k = \frac{\partial f(x_k, u_k)}{\partial x_k} |(x_k, u_k) \\ B_k = \frac{\partial f(x_k, u_k)}{\partial u_k} |(x_k, u_k) \\ C_k = \frac{\partial g(x_k, u_k)}{\partial x_k} |(x_k, u_k) \\ D_k = \frac{\partial g(x_k, u_k)}{\partial u_k} |(x_k, u_k) \end{cases} \tag{8}$$

Combining the equivalent circuit model of the battery and the state equations of the algorithm, the EKF algorithm is implemented as follows:

(1) Initialization state variable $\hat{x}_0$ and state error covariance matrix P_0:

$$\begin{cases} \hat{x}_0 = E(x_0) \\ P_0 = E((x - \hat{x}_0)(x - \hat{x}_0)^T) \end{cases} \tag{9}$$

(2) Update the state variable equation

$$\hat{x}_k^- = f(\hat{x}_{k-1}, u_{k-1}) \tag{10}$$

(3) Update the state error covariance matrix

$$P_k^- = A_{k-1} P_{k-1}^+ A_{k-1}^T + Q_k \tag{11}$$

(4) Calculation of the Kalman gain

$$K_k = \frac{P_k C_k^T}{C_k P_k C_k^T + R_k} \tag{12}$$

(5) Update of the state estimate in the EKF

$$\begin{cases} \hat{y}_k = g(\hat{x}_k, u_k) \\ \hat{x}_k = \hat{x}_{k-1}^- + K_k(y_k - \hat{y}_k) \end{cases} \tag{13}$$

(6) Updated error covariance matrix

$$P_k = (I - K_k C_k) P_k^- \tag{14}$$

In step 5, the sum of the cross time scales Δt_1 and Δt_2 is a cycle to determine whether the total cycle corresponding to the entire battery charge/discharge data has been achieved.

In summary, first of all, it is necessary to determine a small time scale Δt_1, because Δt_1 is too large to lead to more steps in the identification of parameters under complex working conditions, resulting in the proposed algorithm is severely reduced effective. Then the size of time scale Δt_2 is determined for SOC estimation, in general, $\Delta t_1 < \Delta t_2$. Finally, the cell parameters are cross recognized and the cell SOC is estimated during the total time of complex conditions such as DST and FUDS.

4. Experimental validation and discussion

4.1. Dataset description

The method proposed in this paper is validated by using the A123 lithium-ion battery dataset from the Center for Advanced Life Cycle Engineering (CALCE) at University of Maryland [35]. As summarized in Table 4. In the dataset, the battery was operated under full charge and discharge, the sampling time T of current, voltage was 1 s.

Table 4
Details of battery test experiments.

Type	Nominal capacity	Nominal voltage	Voltage ranges
LiFePO4	1100 mAh	3.3 V	3.6 V/2.0 V
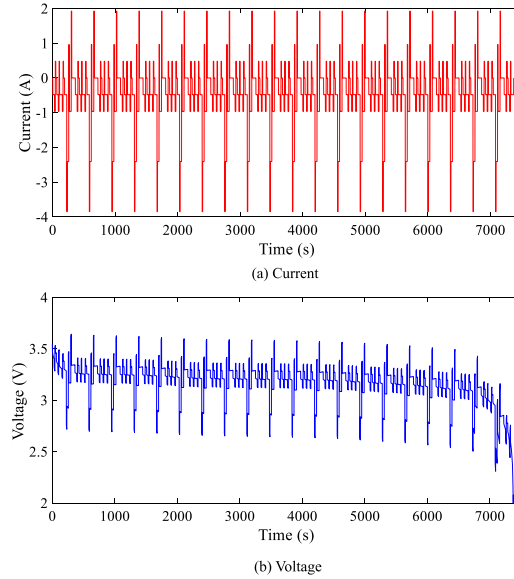
(a) Current

(b) Voltage

Fig. 4. Voltage and current profiles of DST.

For model parameter identification and SOC estimation, the dynamic stress test (DST) and the Federal Urban Driving Schedule (FUDS) was run from -10 °C to 50 °C. DST and FUDS are employed to investigate the dynamic electric behavior of the battery, It is designed by US Advanced Battery Consortium (USABC) to simulate a variable-power discharge regime that represents the expected demands of an EV battery [36]. In this paper, the battery dataset with different operating conditions at the same temperature (DST, FUDS) and the battery dataset with different temperatures at the same operating conditions (-10 °C, 0 °C, 20 °C) are selected as the validation dataset of the proposed algorithm.

4.2. Experimental validation and discussion under different operating conditions at the same temperature

In this section, the experimental validation and discussion of the proposed algorithm are presented under different operating conditions such as DST and FUDS at the same temperature of 25 °C. Fig. 4 displays the voltage and current profiles of DST, while Fig. 5 illustrates voltage and current profiles of FUDS.

From Fig. 4 and Fig. 5, it can be seen that the charging and discharging process exists simultaneously within the DST, FUDS condition, which is more complex compared to the laboratory experiment with only charging or discharging condition. When the traditional FFRLS+EKF algorithm identifies the battery ECM parameters, since the input signals are only voltage and current and the output identifies more parameters, it is bound to bring about jitter or even diffusion of the parameter identification results. Further, the parameter identification results are closely related to the battery SOC estimation accuracy, and when the parameters have jitter, the corresponding SOC estimation accuracy will be affected, which in turn affects the overall SOC estimation accuracy.

Based on the analysis of the aforementioned jitter problem, the proposed algorithm can competently address the jitter problem during the identification of the battery ECM parameters, which ultimately improves the accuracy of the SOC estimation.

In general, MAE and RMSE are both commonly used to assess the model's goodness of fit. The equations for these indicators are as follows.
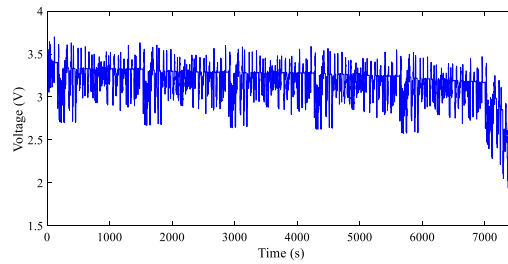
$$MAE = \frac{1}{N} \sum_{i=1}^{N} |\hat{y}_i - y_i| \tag{15}$$

$$RMSE = \sqrt{\frac{1}{N} \sum_{i=1}^{N} (\hat{y}_i - y_i)^2} \tag{16}$$

where N is the number of battery charge/discharge data, $\hat{y}_i$ and y_i are respectively the estimated and true value. The Mean Absolute Error (MAE) quantifies the proximity of forecasts to the corresponding outcomes regardless of the direction. Conversely, the Root
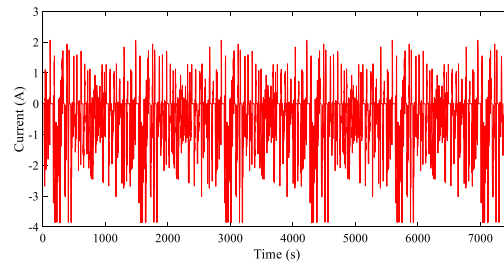
(a) Current

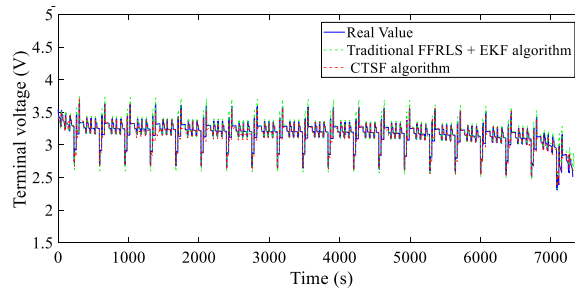(b) Voltage

Fig. 5. Voltage and current profiles of FUDS.

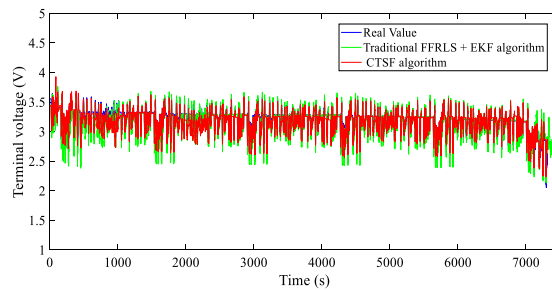**Fig. 6.** The terminal voltage response of DST at 25 °C.

Fig. 7. The terminal voltage response of FUDS at 25 °C.

Mean Square (RMS) Error is highly responsive to substantial errors compared to the Root Mean Square Error (RMSE). It effectively characterizes the level of variation in errors [36].

At the same time, using the input dataset of voltage and current at a constant temperature of 25 °C under both DST and FUDS conditions, the terminal voltage (U_t) is calculated, the ECM parameters of the battery are determined, the SOC is estimated using both the traditional and the proposed algorithms. Fig. 6 shows the terminal voltage results of the proposed and traditional algorithms of DST. Fig. 7 shows the terminal voltage results of the proposed and traditional algorithms of FUDS.

From Fig. 6 and Fig. 7, it can be seen that the terminal voltages obtained by both the proposed algorithm and the conventional algorithm are well fitted to the actual output voltage and the results are given in Table 5 and Table 6. The MAE and RMSE between the estimated and actual terminal voltage values decrease under both DST and FUDS conditions.
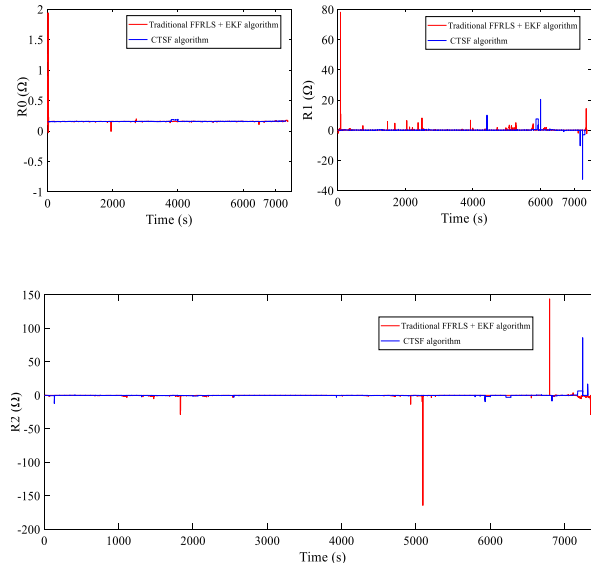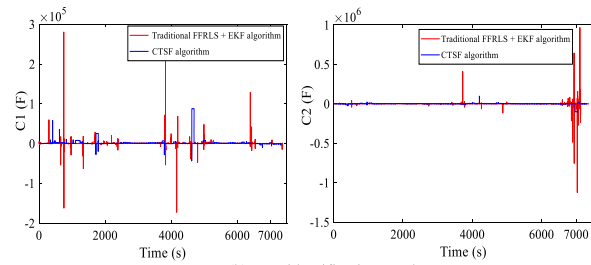
Table 5
Terminal voltage results for DST.

	Traditional algorithm	Proposed algorithm
MAE(%)	3.82	2.28
RMSE(%)	2.79	2.07

Table 6
Terminal voltage results for FUDS.

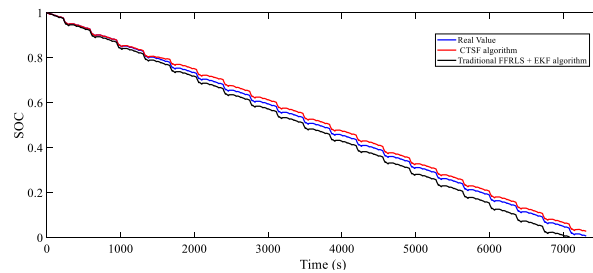|	Traditional algorithm	Proposed algorithm
MAE(%)	5.55	4.51
RMSE(%)	3.55	2.58

(a) $R_0 \sim R_2$ identification results

(b) $C_1 \sim C_2$ identification results

Fig. 8. Comparison of the parameter identification for two algorithms under DST.

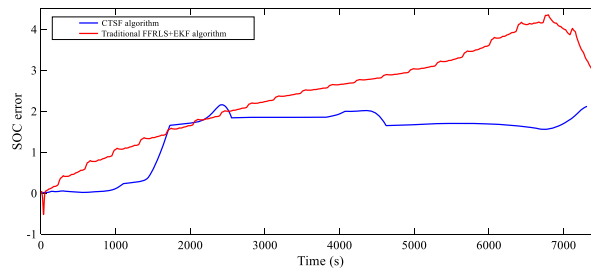**Fig. 9.** Comparison of the estimated SOC for three conditions under DST.

Fig. 10. Comparison of the SOC error for two algorithms under DST.

Table 7
SOC error results of the two algorithms for DST.

	Traditional algorithm	Proposed algorithm
MAE(%)	2.42	1.42
RMSE(%)	2.41	1.42

Table 8
SOC error results of the two algorithms for FUDS.

	Traditional algorithm	Proposed algorithm
MAE(%)	2.17	1.54
RMSE(%)	2.13	1.46

From Fig. 8, it is evident that the traditional algorithm exhibits anomalous jitter in parameter identification during DST conditions. Specifically, parameters C_1 and C_2 reveal extra sources of jitter, while other parameters such as R_1, R_2 display varying degrees of jitter too. However, the proposed algorithm results in a remarkable decrease in the amount of jitters, with only a minor amount of jitters at specific locations.

Fig. 9 illustrates the true SOC values alongside the estimated values obtained from both the traditional algorithm and the proposed algorithm. By analyzing Fig. 9, it is observed that both algorithms have better SOC following characteristics.

Fig. 10 is a comparison of the SOC estimation errors between two algorithms. The MAE and RMSE of the proposed algorithm are reduced by a maximum of 41.3% and 41% compared to the conventional algorithm. The detailed error distribution is shown in Table 7.

Fig. 11 shows the results of parameter identification of the two algorithms under FUDS conditions, for R_0 R_2, the proposed algorithm almost removes the jitters present in the traditional algorithm. For C_1 and C_2, the proposed algorithm also removes most of the jitters, but undeniably, there still exists a small amount of jitters, which is related to the choice of the two time-scale.

Fig. 12 illustrates a comparison between the estimated SOC values obtained from the traditional algorithm and the proposed algorithm. The graph clearly demonstrates that both algorithms converge rapidly and accurately to the approximate true SOC value.

Fig. 13 illustrates the comparison between the proposed algorithm and the traditional algorithm in terms of SOC estimation error. s. The MAE and RMSE of the proposed algorithm are reduced by 29% and 31.4% compared to the conventional algorithm... The detailed error distribution is shown in Table 8.

4.3. Experimental validation and discussion of different temperatures for the same operating condition

In this section, the parameter identification and SOC estimation of the two algorithms at different temperatures (-10 °C, 0 °C, and 25 °C) for the DST condition will be presented.

Fig. 14, Fig. 15 and Fig. 6 compare the results of the terminal voltage for real value, traditional algorithm, proposed algorithm. Fig. 14 shows the estimated results when a dynamic DST test was run at -10 °C, Fig. 15 shows the estimated results when a dynamic DST test was run at 0 °C, Fig. 6 shows the estimated results when a dynamic DST test was run at 25°C. Comparing the fitting of terminal voltages at different temperatures, both the traditional and proposed algorithms can track the curve of the real value of the terminal voltage very well, but there are differences in the error results, Table 9, Table 10 and Table 7 show the results of the terminal errors at -10 °C, 0 °C and 25 °C, respectively.

It can be seen that the MAE and RMSE of the proposed algorithm are reduced to different degrees compared with the traditional algorithm for the DST condition at different temperatures, the MAE is reduced by a maximum of 40.15%, the RMSE is reduced by a maximum of 29.45%. So it shows that the proposed algorithm has good performance in tracking the terminal voltage profile.

Fig. 16, Fig. 17 and Fig. 8 represent the results of identifying the parameters of the battery ECM for the two algorithms at -10 °C, 0 °C and 25 °C, respectively, for the DST condition. In Fig. 16, $R_0 \sim R_2$ in the traditional algorithm parameter identification process, there is a large jitter at the starting position, and some smaller jitters at other positions, while the proposed algorithm eliminates the jitters of $R_0 \sim R_2$ very well. Similarly, the proposed algorithm basically eliminates the more jitters present in the traditional
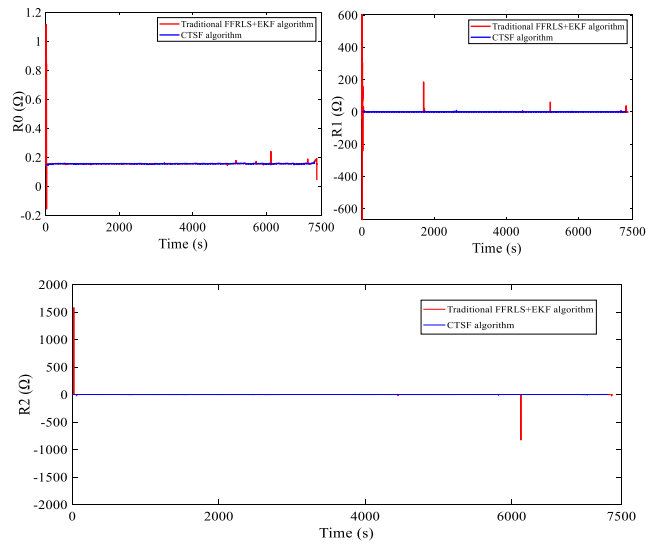
(a) $R_0 \sim R_2$ identification results
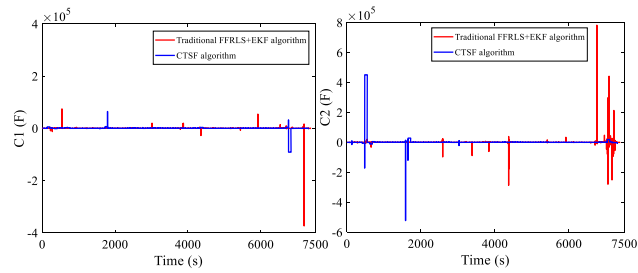
(b) $C_1 \sim C_2$ identification results

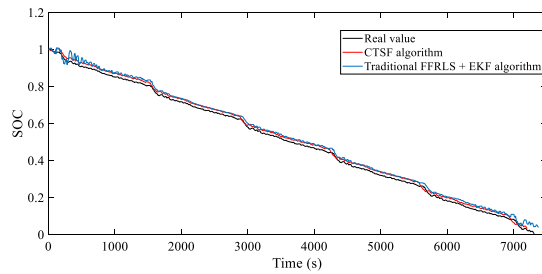**Fig. 11.** Comparison of the parameter identification for two algorithms under FUDS.

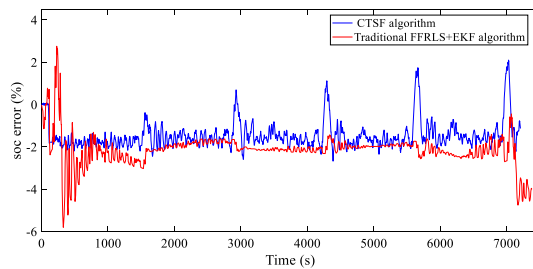**Fig. 12.** Comparison of the estimated SOC for three conditions under FUDS.

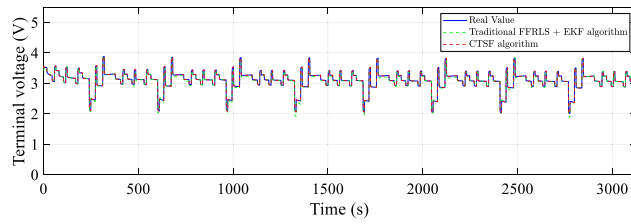**Fig. 13.** Comparison of the SOC error for two algorithms under FUDS.

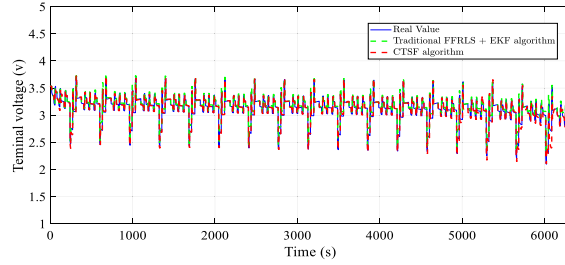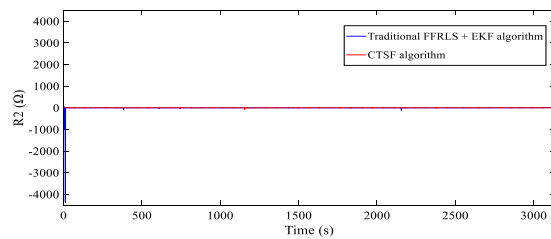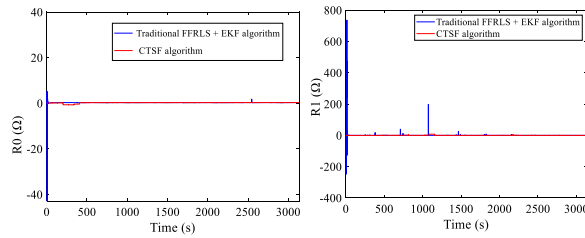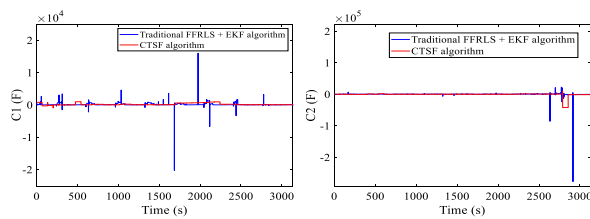**Fig. 14.** The terminal voltage response of DST at -10 °C.

Fig. 15. The terminal voltage response of DST at 0 °C.

(a) $R_0 \sim R_2$ identification results

(b) $C_1 \sim C_2$ identification results

Fig. 16. Comparison of the parameter identification for two algorithms at -10 °C.

Table 9
Terminal voltage results for DST at -10 °C.

	Traditional algorithm	Proposed algorithm
MAE(%)	1.7	1.34
RMSE(%)	1.29	0.91

Table 10
Terminal voltage results for DST at 0 °C.

	Traditional algorithm	Proposed algorithm
MAE(%)	2.29	1.58
RMSE(%)	1.25	0.97

(a) $R_0 \sim R_2$ identification results

(b) $C_1 \sim C_2$ identification results
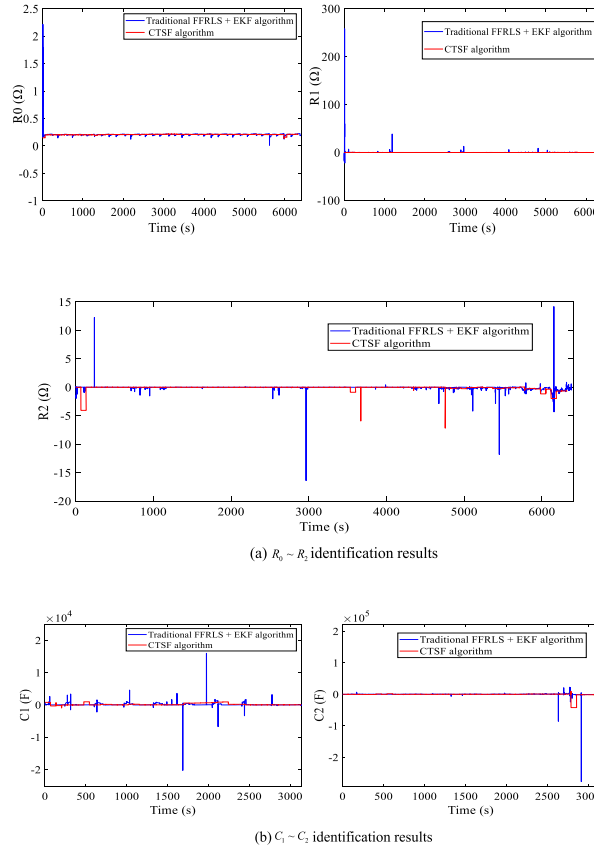
Fig. 17. Comparison of the parameter identification for two algorithms at 0 °C.

algorithm for identifying C_1, C_2, but the proposed algorithm also has less jitters, which is related to the choice of the cross-time scale. In addition, Fig. 17 and Fig. 8 also have better performance in eliminating the jitters.

Fig. 18, Fig. 19, Fig. 9 show the SOC estimation results of the two algorithms for the same DST condition at different temperatures (-10 °C, 0 °C, and 25 °C), respectively. As can be seen from the figures, both algorithms track the true SOC values better, at the same time, the SOC estimation errors are shown in Fig. 20, Fig. 21, Fig. 10, and their MAE, RMSE are listed in Table 11, Table 13, Table 5. Both errors of the proposed algorithm are smaller than the traditional algorithm, which reflects the further improvement in SOC estimation accuracy of the proposed algorithm (Table 12).

In summary, the proposed cross-time-scale algorithm can significantly reduce the jitter of the traditional algorithm for parameter identification at different temperatures and under the same operating conditions, especially for the parameters R_0, R_1, and R_2, which are more effective. The proposed algorithm has only a small amount of jitter at individual locations for only C_1 and C_2 parameters. Additionally, as shown in the Table 13, we summarize the SOC estimation error results of the proposed algorithm for the above working conditions. When the battery model is an equivalent circuit model, comparing Fig. 1 and Fig. 13, the proposed algorithm in this paper has a minimum MAE of 0.22% and a minimum RMSE of 0.3%, which reduces the jitters in the parameter identification and improves the accuracy of SOC estimation at the same time.
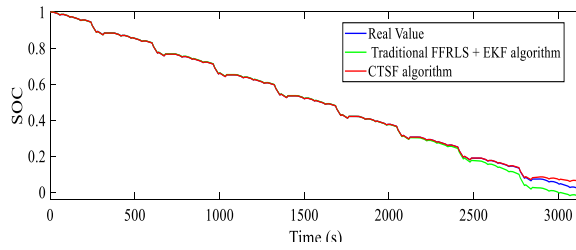
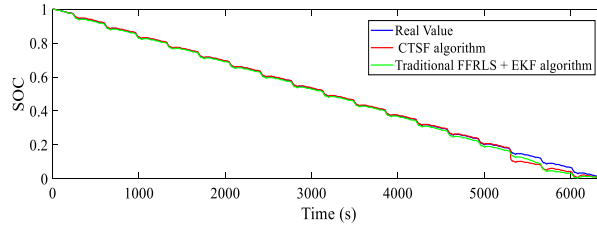**Fig. 18.** Comparison of the estimated SOC for two algorithms at -10 °C.

Fig. 19. Comparison of the estimated SOC for two algorithms at 0 °C.
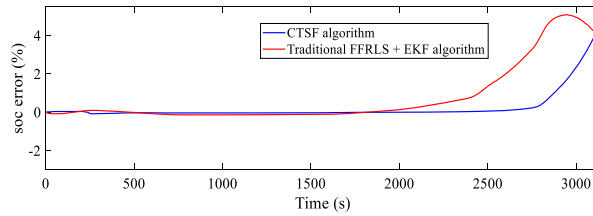
Fig. 20. Comparison of the d SOC error for two algorithms at -10 °C.
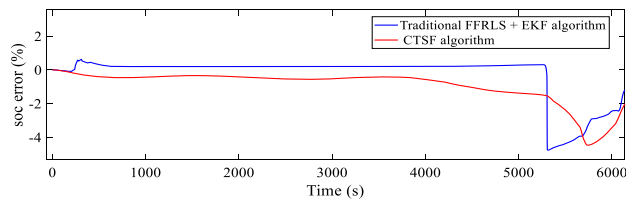
Fig. 21. Comparison of the d SOC error for two algorithms at 0 °C.

Table 11
SOC error results of the two algorithms at -10 °C.

	Traditional algorithm	Proposed algorithm
MAE(%)	0.88	0.25
RMSE(%)	0.78	0.22

Table 12
SOC error results of the two algorithms at 0 °C.

	Traditional algorithm	Proposed algorithm
MAE(%)	0.94	0.66
RMSE(%)	0.92	0.3

Table 13
SOC error results of proposed algorithm.

	MAE(%)	RMSE(%)
DST for 25 °C	1.42	1.42
FUDS for 25 °C	1.54	1.46
DST for 0 °C	0.66	0.3
DST for -10 °C	0.25	0.22

5. Conclusion

Battery parameter identification and SOC estimation are crucial for the proper functioning of batteries. This paper proposes a new method for battery parameter identification and SOC estimation called the cross-time scale fusion algorithm. The main conclusions of this article are as follows.

(1) A cross-time scale fusion algorithm is proposed. The algorithm first determines the cross-times scales Δt_1 and Δt_2, identifies the parameters of the electrical ECM in Δt_1, feeds the results back to Δt_2, and estimates the battery SOC in Δt_2. The parameter identification and SOC estimation are then crossed sequentially.

(2) The algorithm proposed is effective in eliminating the jitter problem, particularly for parameters R_0, R_1, and R_2. However, some jitter still exists during the identification process of parameters C_1 and C_2, which is related to the choice of cross-time scale.

(3) Compared to the traditional FFRLS+EKF algorithm, the proposed algorithm reduces the MAE and RMSE of terminal voltage and SOC to varying degrees under different temperatures for the same operating condition. This demonstrates the proposed algorithm's strong performance across different temperatures.

CRediT authorship contribution statement

Xianzheng Su: Visualization, Validation, Software, Methodology, Formal analysis, Data curation, Conceptualization, Writing – original draft, Writing – review & editing. **Yanjun Ge:** Visualization, Validation, Supervision, Conceptualization, Methodology. **Xin Qiao:** Writing – review & editing, Validation, Supervision, Methodology.

Declaration of competing interest

We declare that we have no financial and personal relationships with other people or organizations that can inappropriately influence our work, there is no professional or other personal interest of any nature or kind in any product, service and/or company that could be construed as influencing the position presented in, or the review of, the manuscript entitled.

Data availability

The data used for the case study in this article is publicly available. Data will be made available on request.

References

[1] Z. Yang, H. Huang, F. Lin, Sustainable electric vehicle batteries for a sustainable world: perspectives on battery cathodes, environment, supply chain, manufacturing, life cycle, and policy, Adv. Energy Mater. 12 (26) (2022) 2200383.
[2] L. Zhang, Q. Qin, China's new energy vehicle policies: evolution, comparison and recommendation, Transp. Res., Part A, Policy Pract. 110 (2018) 57–72.
[3] X. Zhang, Z. Li, L. Luo, Y. Fan, Z. Du, A review on thermal management of lithium-ion batteries for electric vehicles, Energy 238 (2022) 121652.
[4] H. Ren, Y. Zhao, S. Chen, L. Yang, A comparative study of lumped equivalent circuit models of a lithium battery for state of charge prediction, Int. J. Energy Res. 43 (13) (2019) 7306–7315.
[5] M.A. Hannan, M.H. Lipu, A. Hussain, A. Mohamed, A review of lithium-ion battery state of charge estimation and management system in electric vehicle applications: challenges and recommendations, Renew. Sustain. Energy Rev. 78 (2017) 834–854.
[6] L. Sun, G. Li, F. You, Combined internal resistance and state-of-charge estimation of lithium-ion battery based on extended state observer, Renew. Sustain. Energy Rev. 131 (2020) 109994.
[7] Y. Gao, K. Liu, C. Zhu, X. Zhang, D. Zhang, Co-estimation of state-of-charge and state-of-health for lithium-ion batteries using an enhanced electrochemical model, IEEE Trans. Ind. Electron. 69 (3) (2021) 2684–2696.
[8] Y. Song, D. Liu, H. Liao, Y. Peng, A hybrid statistical data-driven method for on-line joint state estimation of lithium-ion batteries, Appl. Energy 261 (2020) 114408.
[9] H. Dai, B. Jiang, X. Hu, X. Lin, X. Wei, M. Pecht, Advanced battery management strategies for a sustainable energy future: multilayer design concepts and research trends, Renew. Sustain. Energy Rev. 138 (2021) 110480.
[10] M.H. Lipu, M. Hannan, A. Hussain, A. Ayob, M.H. Saad, T.F. Karim, D.N. How, Data-driven state of charge estimation of lithium-ion batteries: algorithms, implementation factors, limitations and future trends, J. Clean. Prod. 277 (2020) 124110.
[11] W. Zhou, Y. Zheng, Z. Pan, Q. Lu, Review on the battery model and soc estimation method, Processes 9 (9) (2021) 1685.
[12] Y. Zheng, M. Ouyang, X. Han, L. Lu, J. Li, Investigating the error sources of the online state of charge estimation methods for lithium-ion batteries in electric vehicles, J. Power Sources 377 (2018) 161–188.
[13] X. Lin, Y. Tang, J. Ren, Y. Wei, State of charge estimation with the adaptive unscented Kalman filter based on an accurate equivalent circuit model, J. Energy Storage 41 (2021) 102840.
[14] H.Y. Pai, Y.H. Liu, S.P. Ye, Online estimation of lithium-ion battery equivalent circuit model parameters and state of charge using time-domain assisted decoupled recursive least squares technique, J. Energy Storage 62 (2023) 106901.

[15] Z. He, Z. Yang, X. Cui, E. Li, A method of state-of-charge estimation for ev power lithium-ion battery using a novel adaptive extended Kalman filter, IEEE Trans. Veh. Technol. 69 (12) (2020) 14618–14630.

[16] J. Chen, Y. Zhang, J. Wu, W. Cheng, Q. Zhu, Soc estimation for lithium-ion battery using the lstm-rnn with extended input and constrained output, Energy 262 (2023) 125375.

[17] F. Mohammadi, Lithium-ion battery state-of-charge estimation based on an improved Coulomb-counting algorithm and uncertainty evaluation, J. Energy Storage 48 (2022) 104061.

[18] Y.-X. Wang, Z. Chen, W. Zhang, Lithium-ion battery state-of-charge estimation for small target sample sets using the improved gru-based transfer learning, Energy 244 (2022) 123178.

[19] X. Ren, S. Liu, X. Yu, X. Dong, A method for state-of-charge estimation of lithium-ion batteries based on pso-lstm, Energy 234 (2021) 121236.

[20] X. Feng, J. Chen, Z. Zhang, S. Miao, Q. Zhu, State-of-charge estimation of lithium-ion battery based on clockwork recurrent neural network, Energy 236 (2021) 121360.

[21] C. Ge, Y. Zheng, Y. Yu, State of charge estimation of lithium-ion battery based on improved forgetting factor recursive least squares-extended Kalman filter joint algorithm, J. Energy Storage 55 (2022) 105474.

[22] X. Chen, H. Lei, R. Xiong, W. Shen, R. Yang, A novel approach to reconstruct open circuit voltage for state of charge estimation of lithium ion batteries in electric vehicles, Appl. Energy 255 (2019) 113758.

[23] Y. Wang, D. Meng, Y. Chang, Y. Zhou, R. Li, X. Zhang, Research on online parameter identification and soc estimation methods of lithium-ion battery model based on a robustness analysis, Int. J. Energy Res. 45 (15) (2021) 21234–21253.

[24] X. Qin, T. Hao, J. Ding, Multi-measurement Kalman-filtering-based neural network estimator for soc of lithium batteries, J. Electrochem. Soc. 170 (12) (2023) 120517.

[25] M.R. Ramezani-al, M. Moodi, A novel combined online method for soc estimation of a Li-ion battery with practical and industrial considerations, J. Energy Storage 67 (2023) 107605.

[26] Q. Wang, M. Ye, M. Wei, G. Lian, Y. Li, Deep convolutional neural network based closed-loop soc estimation for lithium-ion batteries in hierarchical scenarios, Energy 263 (2023) 125718.

[27] X. Fan, W. Zhang, C. Zhang, A. Chen, F. An, Soc estimation of Li-ion battery using convolutional neural network with u-net architecture, Energy 256 (2022) 124612.

[28] P. Qin, L. Zhao, A novel transfer learning-based cell soc online estimation method for a battery pack in complex application conditions, IEEE Trans. Ind. Electron. (2023).

[29] R. Guo, C. Hu, W. Shen, An adaptive approach for battery state of charge and state of power co-estimation with a fractional-order multi-model system considering temperatures, IEEE Trans. Intell. Transp. Syst. (2023).

[30] X. Liu, K. Li, J. Wu, Y. He, X. Liu, An extended Kalman filter based data-driven method for state of charge estimation of Li-ion batteries, J. Energy Storage 40 (2021) 102655.

[31] P. Macklin, S. McDougall, A.R. Anderson, M.A. Chaplain, V. Cristini, J. Lowengrub, Multiscale modelling and nonlinear simulation of vascular tumour growth, J. Math. Biol. 58 (2009) 765–798.

[32] X. Qiao, Z. Wang, E. Hou, G. Liu, Y. Cai, Online estimation of open circuit voltage based on extended Kalman filter with self-evaluation criterion, Energies 15 (12) (2022) 4373.

[33] A. Barai, G.H. Chouchelamane, Y. Guo, A. McGordon, P. Jennings, A study on the impact of lithium-ion cell relaxation on electrochemical impedance spectroscopy, J. Power Sources 280 (2015) 74–80.

[34] Z. Ren, C. Du, Z. Wu, J. Shao, W. Deng, A comparative study of the influence of different open circuit voltage tests on model-based state of charge estimation for lithium-ion batteries, Int. J. Energy Res. 45 (9) (2021) 13692–13711.

[35] Y. Xing, E.W. Ma, K.-L. Tsui, M. Pecht, An ensemble model for predicting the remaining useful performance of lithium-ion batteries, Microelectron. Reliab. 53 (6) (2013) 811–820.

[36] Y. Xing, W. He, M. Pecht, K.L. Tsui, State of charge estimation of lithium-ion batteries using the open-circuit voltage at various ambient temperatures, Appl. Energy 113 (2014) 106–115.